Recep Tayyip Erdoğan Üniversitesi Fen ve Mühendislik Bilimleri Dergisi, 6(1) 14-31 2025
Recep Tayyip Erdogan University Journal of Science and Engineering, 6(1) 14-31 2025
ISSN: 2687-2315 / E-ISSN: 2757-7686

Energy Levels and Absorption Coefficients for Diverse Bounded Potentials: A Comprehensive Analysis

Tərlan ZƏRBALİYEV [1], Raşit ÇAKIR [2*], Hasan YILDIRIM [3]

[1]Department of Advanced Technologies, Institute of Graduate Studies, Recep Tayyip Erdogan University, Rize, Türkiye

[2]Physics Department, Faculty of Arts and Sciences, Recep Tayyip Erdogan University, Rize, Türkiye

[3]Department of Occupational Health and Safety, Faculty of Health Sciences, Karabuk University, Karabuk, Türkiye

Sorumlu Yazar/Corresponding Author
E-mail: rasit.cakir@erdogan.edu.tr

Araştırma Makalesi/Research Article
Geliş Tarihi/Received: 05.03.2024
Kabul Tarihi/Accepted: 07.02.2025

Abstract

This article presents a comprehensive numerical investigation into the energy levels and absorption coefficients within quantum well structures, with a particular focus on the GaAs/AlGaAs system. Various bounded potentials, including the Rosen-Morse potential, Wood-Saxon potential, Pöschl-Teller potential, Razavy potential, inversely quadratic Hellmann potential, Kratzer-Fues potential, and Morse potential, are explored. Employing the Schrödinger equation, with considerations for effective mass and envelope function approximations, a discrete formulation is attained through finite differences. Throughout the analysis, the effective mass ratio is upheld as a constant value characteristic of GaAs. The study reveals that transition energies and absorption coefficients exhibit subtle variations in response to alterations in well parameters, spanning from the lower bounds of the near-infrared spectrum to the midpoints of the far-infrared region. By comprehensively studying these phenomena across a spectrum of potentials, this research contributes valuable insights into the behavior and characteristics of quantum well structures, particularly within the context of the GaAs/AlGaAs system.

Keywords: Quantum well, intersubband absorption, GaAs, finite difference method

Çeşitli Bağlı Potansiyeller için Enerji Seviyeleri ve Soğurma Katsayıları: Kapsamlı Bir Analiz

Öz

Bu makale, GaAs/AlGaAs sistemi üzerinde odaklanarak kuantum kuyu yapıları içindeki enerji seviyeleri ve soğurma katsayıları üzerine kapsamlı bir sayısal incelemeyi sunmaktadır. Rosen-Morse potansiyeli, Wood-Saxon potansiyeli, Pöschl-Teller potansiyeli, Razavy potansiyeli, ters kuadratik Hellmann potansiyeli, Kratzer-Fues potansiyeli ve Morse potansiyeli gibi çeşitli bağlı potansiyeller keşfedilmektedir. Etkin kütle ve zarf fonksiyonu yaklaşımlarını dikkate alarak, Schrödinger denklemi, sonlu farklar kullanılarak bir ayrık forma dönüştürülür. Analiz boyunca, etkin kütle oranı GaAs'ın karakteristik bir sabit değeri olarak tutulmuştur. Çalışma, kuyu parametrelerindeki değişikliklere karşı geçiş enerjileri ve emilim katsayılarının ince farklılıklar sergilediğini ortaya koymaktadır. Bu, yakın kızılötesi spektrumun alt sınırlarından uzak kızılötesi bölgenin ortalarına kadar uzanır. Farklı potansiyeller yelpazesinde bu fiziksel olayları kapsamlı bir şekilde inceleyerek, özellikle GaAs/AlGaAs sistemi bağlamında, bu araştırma kuantum kuyu yapılarının davranışı ve özellikleri hakkında değerli görüşler sunmaktadır.

Anahtar Kelimeler: Kuantum kuyusu, ara-altı bant soğurumu, GaAs, sonlu farkla yöntemi

Cite as;
Zərbaliyev, T., Çakır, R., Yıldırım, H. (2025). Energy levels and absorption coefficients for diverse bounded potentials: A comprehensive analysis. *Recep Tayyip Erdogan University Journal of Science and Engineering*, 6(1), 14-31. Doi: 10.53501/rteufemud.1446402

1. Introduction

The study of quantum well structures has been a focal point in solid-state physics and materials science, driven by their exceptional properties and their pivotal role in modern electronic and optoelectronic devices. Quantum wells are epitomized by their two-dimensional confinement of charge carriers, resulting in discrete energy levels that give rise to unique electronic properties. The choice of potential governing the behavior of carriers within these quantum wells significantly influences the resulting energy spectrum and optical properties. In the design of semiconductor devices, such as lasers, photodetectors, and quantum cascade devices, the absorption coefficient is a fundamental parameter. It determines how efficiently the material can absorb incident photons, which is essential for the operation of these devices. The absorption coefficient directly influences the device's performance, including its efficiency and sensitivity.

Quantum wells are important for improving mid-infrared and terahertz technologies. Research is focused on optimizing intersubband transitions in semiconductor quantum wells to create lasers that work at specific wavelengths. These transitions are essential for laser efficiency, and scientists are working to improve the processes that generate light. Similarly, nonradiative processes, like phonon interactions and scattering, affect performance, so efforts are being made to reduce these issues. Current studies aim to improve thermal management, efficiency, and power use while expanding the range of wavelengths. New materials and design innovations are helping quantum cascade lasers become more effective for applications in sensing, communication, and spectroscopy (Atić et al., 2022, 2024; Cominotti 2023; Khurgin 2023).

In this study, we delve into the comprehensive analysis of the single $GaAs/AlGaAs$ quantum well structures, aiming to explore their energy levels and absorption coefficients when subjected to a range of bounded potentials. We have considered seven distinctive potentials, each characterized by different parameter values. The potential functions are as follows: 1) Rosen-Morse potential, 2) Wood-Saxon potential, 3) Pöschl-Teller potential, 4) Razavy potential, 5) inversely quadratic Hellmann potential, 6) Kratzer-Fues potential and 7) Morse potential. Experimental studies use the potentials directly or apply them to various quantum systems, molecular interactions, and resonance phenomena. Although many experimental studies might not exclusively focus on these potentials, they are often applied as effective models in various fields, especially in atomic, molecular, nuclear, and quantum physics research. Quantum well intersubband absorptions are crucial for enabling precise control of light-matter interactions at specific wavelengths, making them essential for advanced optoelectronic applications like quantum cascade lasers and infrared detectors. (Persichetti et al., 2020).

2. Material and Method

We consider a single quantum well structure having the potential $U(z)$. The Hamiltonian for the electrons inside the potential $U(z)$ within the effective mass and envelope function approximation is

$$H = -\frac{\hbar^2}{2m^*}\left(\frac{\partial^2}{\partial x^2}+\frac{\partial^2}{\partial y^2}+\frac{\partial^2}{\partial z^2}\right)+\ U(z) \qquad (1)$$

where m^* is the effective mass and $\hbar$ is the reduced Planck's constant. We chose z as the growth direction. The energy eigenvalues $E_{n,k}$ and eigenfunctions $\psi_{n,k}$ for this Hamiltonian are given as

$$E_{n,k} = E_n + \frac{\hbar^2}{2m^*}\left|\boldsymbol{k}_{\parallel}\right|^2 \tag{2}$$

$$\psi_{n,k}(\boldsymbol{r}) = \psi_n(z)\exp(i\,\boldsymbol{k}_{\parallel}\cdot\boldsymbol{r}_{\parallel}) \tag{3}$$

where $\boldsymbol{k}_{\parallel}$ and $\boldsymbol{r}_{\parallel}$ are the wave and position vectors in the $x-y$ plane, and E_n is the energy and $\psi_n(z)$ is the wave function of the n -th sub-band in the z growth direction (Flügge, 1999). We solve numerically the time independent Schrödinger equation

$$H_z\psi_n(z) = -\frac{\hbar^2}{2m^*}\frac{\partial^2}{\partial z^2}\psi_n(z) + U(z)\psi_n(z) = E_n\psi_n(z) \tag{4}$$

in the growth direction, where H_z is the z component of the Hamiltonian.

The Schrödinger equation is discretized by means of finite differences and the eigenvalues and eigenfunctions of the resulting matrix equation give the energy values and corresponding wave functions (Harrison, 2005). We consider z in units of Ångströms (Å) and energy in millielectronvolts (meV). The effective mass is defined as $m^* = mm_0$, where m_0 is the electron mass and $m = 0.067$ is the electron's effective mass ratio for GaAs. Replacing $(z \to z10^{-10})$, $(E_n \to e10^{-3}E_n)$ and $(U \to e10^{-3}U)$, the Schrödinger equation takes a numerically solvable form.

$$-\frac{M}{m}\frac{\partial^2}{\partial z^2}\psi_n(z) + U(z)\psi_n(z) = E_n\psi_n(z) \tag{5}$$

where $M = \hbar^2 10^{23}/(2m_0 e)$. No unit conversion is required for the wave function because multiplying the wave function by a constant does not affect the form of the equation.

The position variable z is partitioned into N intervals. The indices will change as $i = 0, 1, 2, \ldots N$ and the z_i values can be obtained from the given position range. The second order derivative will be numerically calculated as follows.

$$\frac{\partial^2}{\partial z^2}\psi(z) \approx \frac{1}{(\Delta z)^2}(\psi_{i+1} - 2\psi_i + \psi_{i-1}) \tag{6}$$

where Δz is the increment of space and $\psi_i = \psi(z_i)$ are the unknown variables. By substituting this into the Schrödinger equation and using $U_i = U(z_i)$, we obtain $(N+1)$ equations with $(N+1)$ unknowns of ψ_i, where the ith equation is as below.

$$-\frac{2M}{m(\Delta z)^2}\psi_{i-1} + \left(\frac{2M}{m(\Delta z)^2} + U_i\right)\psi_i - \frac{2M}{m(\Delta z)^2}\psi_{i+1} = E\psi_i \tag{7}$$

We also apply the boundary conditions $\psi_{-1} = 0$ for $n = 0$ at the first equation and $\psi_{N+1} = 0$ for $n = N$ at the last one, which introduces negligible numerical error since ψ in a bounded potential approaches zero at both boundaries. These $(N + 1)$ equations can be written as a matrix equation.

$$[\mathrm{A}]_{(N+1)\times(N+1)}[\Psi]_{(N+1)\times 1} = E[\Psi]_{(N+1)\times 1} \tag{8}$$

where Ψ is the diagonal matrix of the unknown ψ_i values and A is a tridiagonal square matrix with the elements specified below.

$$A_{i,i} = \frac{2M}{m(\Delta z)^2} + U_i \quad \text{and} \quad A_{i,i\pm1} = -\frac{2M}{m(\Delta z)^2} \tag{9}$$

We numerically solve the eigenvalue equation for the symmetric square matrix A and obtain the $(N + 1)$ number of eigenvalues for the energies E and the corresponding eigenfunctions of ψ. However, only the energy values that are less than the maximum potential value have physical significance. From the calculated energies and wave functions, we calculate the absorption coefficient. The first order linear absorption coefficients derived by using the density matrix formalism and perturbation expansion method is given as

$$\alpha^{(1)}(\omega) = \frac{\omega}{n_r c \varepsilon_0} |\mu_{10}|^2 \frac{\sigma_s \hbar \Gamma_0}{(E_{10} - \hbar\omega)^2 + (\hbar\Gamma_0)^2} \tag{10}$$

where $|\mu_{10}| = e|\langle\psi_1|z|\psi_2\rangle|$ is the dipole matrix element and $E_{10} = E_1 - E_0$ is the energy difference of the ground and first excited states, σ_s is the electron density in the well, Γ_0 is the inverse of the relaxation time, $n_r = \sqrt{\varepsilon_r}$ is the refractive index of the well, ω is the frequency of the incident light, ε_0 is the vacuum permittivity, and c is the speed of light in vacuum (Ahn and Chuang, 1987; Yıldırım and Tomak, 2005).

We consider the $\mathrm{GaAs/Al_xGa_{1-x}As}$ quantum well structures, where $0 \leq x \leq 1$ is the Al concentration. The band gap of $\mathrm{Al_xGa_{1-x}As}$ increases with the concentration x so the shape of the potential will change with $x = x(z)$. The concentration dependence of the well potential is given as $U(x) = 0.67\Delta E_g = 835.49x$ (meV), where ΔE_g is the band gap energy difference between $\mathrm{Al_xGa_{1-x}As}$ and GaAs, and the conduction band offset is 67% (Harrison, 2005). Even though the maximum well potential cannot be more than 835.46 meV , this is ignored in some potentials. The Al concentration over well distance will change as $x(z) = U(z)/835.49$ for a given $U(z)$ potential. In all calculations, the effective mass ratio is taken as the constant value of $m^* = 0.067$ for all concentrations and the increment of space is taken as $\Delta z = 1$. All numerical calculations are performed by using the SciPy Stack (van der Walt et al., 2011).

3. Results and Discussions

3.1 Rosen-Morse Potential

This potential is frequently applied in molecular and chemical physics to model the vibrational spectra of diatomic molecules, especially near equilibrium bond lengths. Its shape can capture the subtle behavior of electron movement within a molecular bond, making it useful for spectroscopy and the study of molecular interactions. It was introduced by Rosen and Morse to explore vibrational energies in polyatomic molecules (Rosen and Morse, 1932). The Rosen–Morse confinement profile has garnered significant attention for its diverse applications across various physics disciplines. Subsequently, numerous analytical techniques have been developed to study the Rosen–Morse confinement profile, reflecting its importance and versatility in theoretical investigations (Khordad and Mirhosseini, 2014; Salman Durmuslar et al., 2022; Haghighatzadeh and Attarzadeh, 2023). The hyperbolic Rosen-Morse potential is given as

$$U(z) = U_0 \tanh^2\left(\frac{z}{\eta}\right) \tag{11}$$

where U_0 and η are constants (Ungan and Bahar, 2019, 2020). The potential minimum is zero at $z = 0$ and U_0 is the barrier potential. The well width and depth are scaled with η and U_0, respectively. The potential energy profile and the squared wave functions of the ground and first excited states are shown in

Figure **1**(c) for $\eta = 20$ Å, $\eta = 25$ Å and $\eta = 30$ Å . The barrier potential is $U_0 = 835.49$ meV for AlAs. The z range is taken as $[-250$ Å$, 250$ Å$]$ in the calculations. Energy values of the bounded states are given in

Table **1**. As the parameter η increases, the potential energy profile becomes wider and therefore the quantum well admits more energy levels as shown in Table 1. Accordingly, the energy values of the two lowest subbands get closer; the transition energy between them drops from 419.4 meV to 337.4 meV.

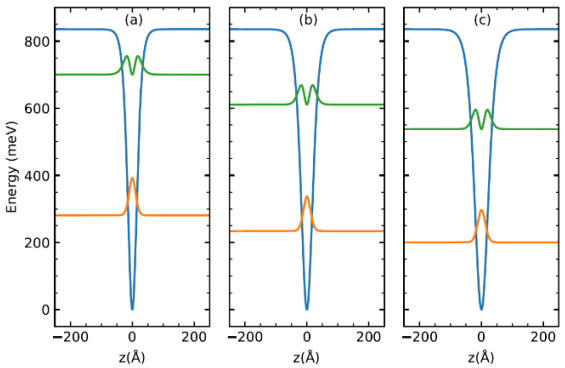

Figure 1 The potential energy profile (blue) and the squared wave functions of the ground (orange) and first excited (green) states of the Rosen-Morse potential for $U_0 = 835.49$ meV and (a) $\eta = 20$ Å , (b) $\eta = 25$ Å and (c) $\eta = 30$ Å

Table 1. Energy values of the Rosen-Morse potential for $U\_0 = 835.49$ meV and for $\eta =$ 20 "Å" , $\eta =$ 25 "Å" and $\eta = 30$ "Å"

n	E_n (meV) for $\eta = 20$ Å	E_n (meV) for $\eta = 25$ Å	E_n (meV) for $\eta = 30$ Å
0	280.75	233.90	200.29
1	700.15	610.73	537.69
2	-	805.72	748.79
3	-	-	834.88

3.2 Wood-Saxon Potential

This potential is known for its application in nuclear physics, where it models the distribution of nuclear forces within an atomic nucleus. It is particularly valuable for studying nuclear shell structures, and it can be applied in nuclear energy and radioactive decay research, where precise models of nucleon behavior are essential. It was introduced by Woods and Saxon to investigate the elastic scattering of protons by heavy nuclei (Woods and Saxon, 1954). The Woods–Saxon potential has proven to be a viable choice for nuclear shell models, drawing significant attention in the field of nuclear physics. It is widely employed for its effectiveness in representing the distribution of nuclear densities, making it a valuable tool for studying various aspects of nuclear structure and interactions (Xie, 2009).

The Wood-Saxon potential is given as

$$U(z) = \frac{U_0}{1 + \exp[(Z_0 - z)/\gamma]} + \frac{U_0}{1 + \exp[(Z_0 + z)/\gamma]} \quad (12)$$

where U_0 is the barrier potential and Z_0 is a constant changing well width (Restrepo et al., 2015; Ungan et al., 2019). The slope of the barriers increases with $\gamma > 0$. When $\gamma \to 0$, the well shape approaches to the finite square well potential. The potential energy profile and the squared wave functions of the ground and first excited states are shown in Figure 2 for $\gamma = 0.1$ Å, $\gamma = 10$ Å and $\gamma = 20$ Å. The barrier potential is $U_0 = 835.49$ meV for AlAs and $Z_0 = 50$ Å. The z range is taken as $[-250\ \text{Å}, 250\ \text{Å}]$ in the calculations. Energy values of the bounded states are given in Table **2**. The parameter γ makes the Wood-Saxon potential energy profile wider and shallower as it becomes larger as shown in Figure 2. However, the bottom part ceases to be flat and the potential energy profile becomes narrower toward it. That yields initially an enhanced transition energy, from 122.5 meV to 174 meV as shown in Table 2. However, as discussed above, the widening profile with the parameter γ lowers the transition energy to 164.97 meV.

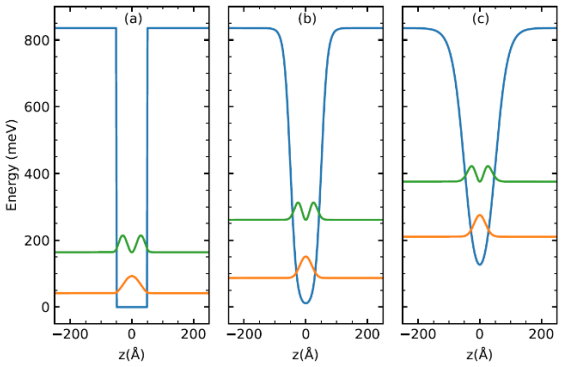

Figure 2 The potential energy profile (blue) and the squared wave functions of the ground (orange) and first excited (green) states of the Wood-Saxon potential for $U_0 = 835.49\ meV$, $Z_0 = 50\ Å$ and (a) $\gamma = 0.1$ Å, (b) $\gamma = 10$ Å and (c) $\gamma = 20$ Å

Table 2. Energy values of the Wood-Saxon potential for $U\_0 = 835.49$ meV, $Z\_0 = 50$ "Å" and for $\gamma = 0.1$ "Å", $\gamma = 10$ "Å" and $\gamma = 20$ "Å"

n	E_n (meV) for $\gamma = 0.1$ Å	E_n (meV) for $\gamma = 10$ Å	E_n (meV) for $\gamma = 20$ Å
0	41.27	86.85	210.68
1	163.78	260.85	375.65
2	362.66	463.24	529.84
3	624.06	660.34	663.46
4	-	808.06	766.37
5	-	-	827.21

3.3 Pöschl-Teller Potential

This potential is used in quantum mechanics and optical physics, especially for problems with solvable quantum systems and in describing solitons in nonlinear optics. Its solvability makes it ideal for teaching purposes and for analytically modeling quantum wells in solid-state physics. It was originally proposed by Pöschl and Teller, and its initial purpose was to model the vibrational behavior of diatomic molecules in the realm of quantum mechanics (Pöschl and Teller, 1933). Over time, it has found extensive application in the examination of both linear and nonlinear optical properties of quantum wells (Yıldırım and Tomak, 2005, 2006; Aytekin et al. , 2012). Numerous researchers have utilized the trigonometric Pöschl-Teller potential as a valuable tool in their studies within the realm of quantum optics and optical properties of various physical systems (Hamzavi and Rajabi, 2011; Falaye, 2012).
The Pöschl-Teller potential is given as

$$U(z) = \frac{\hbar^2\beta^2}{2m^*}\left[\frac{k(k-1)}{\sin^2(\beta z)} + \frac{\eta(\eta-1)}{\cos^2(\beta z)}\right] \tag{13}$$

where $\hbar$ is the reduced Planck's constant, m^* is the effective mass, $k > 1$ and $\eta > 1$ are constants, $\beta = \pi/(2L)$ and L is well width. The potential energy profile and the squared wave functions of the ground and first excited states are shown in Figure 3 for $\eta = 2$ and $k = 1.2$, for $\eta = 2$ and $k = 2$, and for $\eta = 2$ and $k = 3$. When $\eta = k$ the potential becomes symmetric. The potential function has vertical asymptotes at $z = 0$ and $z = L$ so it is an infinite potential. Energy values of the first 4 bounded states are given in Table 3. The bottom part of the Pöschl-Teller potential energy profile is shifted upward and becomes narrower as the parameter k increases from 1.2 to 3 as shown in Figure 3. That makes the transition energy between the lowest two level larger; it increases from 235.48 meV to 336.53 meV. A consequence of the change in the parameter k is that the symmetry of the potential energy profile can be distorted. As shown in Figure 3, while the value $k = 1.2$ gives a profile whose minimum is shifted to the left, the value $k = 3$ gives another one whose minimum is shifted to the right. But when the parameter is set to 2, a symmetric profile is obtained.

Table 3. Energy values of the Pöschl-Teller potential for $L = 100$ Å, $\eta = 2$ and $k = 1.2$ $k = 2$ and $k = 3$

n	E_n (meV) for $k = 1.2$	E_n (meV) for $k = 2$	E_n (meV) for $k = 3$
0	143.61	224.47	350.74
1	379.09	504.92	687.27
2	726.42	897.25	1135.61
3	1185.27	1401.11	1695.38

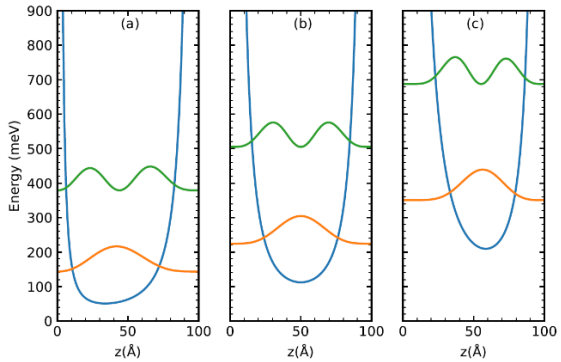

Figure 3 The potential energy profile (blue) and the squared wave functions of the ground (orange) and first excited (green) states of the Pöschl-Teller potential for $L = 100$ Å, $\eta = 2$ and (a) $k = 1.2$, (b) $k = 2$ and (c) $k = 3$

3.4 Razavy Potential

This potential is suitable for modeling double-well potentials and quantum tunneling effects, which have applications in semiconductor technology and chemical reaction dynamics. It is often used in quantum field theory and nonlinear dynamics. It is especially useful for examining symmetry-breaking effects in field theory. This potential was proposed by Razavy as a bistable potential (Razavy, 1980). This potential has found widespread application in molecular physics as an approximate model for characterizing the movement of a particle subjected to the influence of two force centers (Finkel et al. 1999; Sous, 2007).

The Razavy potential is given as

$$U(z) = U_0 \left[A \cosh\left(\frac{z}{D}\right) - M\right]^2 \qquad (14)$$

where U_0, A, D and M are constants (Kasapoglu et al., 2021; Sayrac et al. 2022). When $A > M$, it is a single well with the minimum at $z = 0$. When $A < M$, it is a double well with minimums at $z_\pm = \pm D \operatorname{arccosh}(M/A)$ and the local maximum at $z = 0$. It is an infinite potential but it is not bounded. The potential energy profile and the squared wave functions of the ground and first excited states are shown in Figure 4 for $A = 2$ and $M = 1$, for $A = 2$ and $M = 2$, and for $A = 2$ and $M = 3$ values. The other constants are taken as $U_0 = 300$ meV and $D = 50$ Å. Energy values of the first 4 bounded states are given in Table 4. According to Figure 4, the parameter M gives us wider and deeper potential energy profiles for Razavy potential as it increases and eventually splits the potential energy profile into two parts, and so the parameter creates a potential energy profile of a double quantum well. The corresponding transition energies of the single wells for the lowest two subbands decrease from 267.16 to 153.87 meV, and the double well has the energies of $E_{10} = 15.95$ meV and $E_{21} = 203.48$ meV.

Table 4. Energy values of the Razavy potential for $U\_0 = 300$ meV, $D = 50$ Å, $A = 2$ and $M = 1$, $M = 2$ and $M = 3$

n	E_n (meV) for $M = 1$	E_n (meV) for $M = 2$	E_n (meV) for $M = 3$
0	425.79	58.94	158.80
1	692.95	212.82	174.76
2	988.75	421.92	378.24
3	1309.14	665.87	520.79

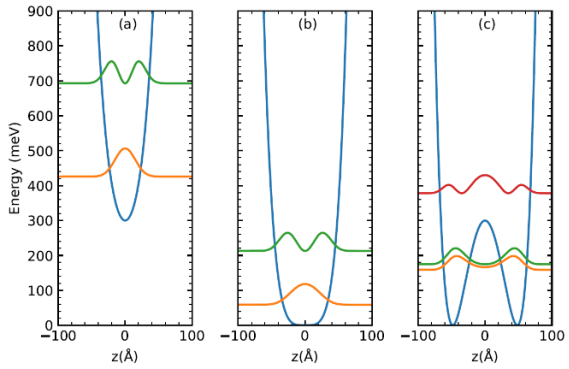

Figure 4 The potential energy profile (blue) and the squared wave functions of the ground (orange), first excited (green) and second excited (red) states of the Razavy potential for $U_0 = 300$ meV , $D = 50$ Å , $A = 2$ and (a) $M = 1$, (b) $M = 2$ and (c) $M = 3$

3.5 Inversely Quadratic Hellmann Potential

This potential is used to approximate Coulombic interactions and long-range intermolecular forces in applied atomic and molecular physics. It can aid in studying ionized gases and plasmas, where particles experience varying degrees of electric interaction, as well as in modeling Rydberg states in highly excited atoms. It finds application in certain physical models aimed at describing particle interactions (Hellmann, 1936). The unique form of this potential enables its application in describing the complex dynamics involved in the interaction between particles in various physical systems (Máthé et al., 2021; Duan et al, 2022; Ghanbari, 2023; Njoku et al, 2023).

The inversely quadratic Hellmann potential is given as

$$U(z) = U_0\left[-\frac{\eta}{z} + \frac{\eta^2}{z^2}\exp\left(-\frac{z}{\eta}\right)\right] \qquad (15)$$

where U_0 and η are constants (Turkoglu et al. 2021). The potential minimum can be numerically calculated as $U_{min} \approx -0.635U_0$ at $z_{min} \approx 1.06\eta$. The well width and depth are scaled with η and U_0, respectively. The potential energy profile and the squared wave functions of the ground and first excited states are shown in Figure 5 for $U_0 = 300$ meV and for $\eta = 50$ Å , $\eta = 100$ Å and $\eta = 200$ Å . The z values is taken until 10^4 Å in the calculations because of the horizontal asymptote at $U = 0$. Energy values of the bounded states are given in Table 5. As the parameter η increases, the potential energy profile expands. Consequently, the energy values of the lowest two subbands approach each other; the transition energy between them decreases from 58.25 meV to 27.72 meV.

Table 5. Energy values of the inversely quadratic Hellmann potential for $U_0 = 300$ meV and $\eta = 50$ Å, $\eta = 100$ Å and $\eta = 200$ Å

n	E_n (meV) for $\eta = 50$ Å	E_n (meV) for $\eta = 100$ Å	E_n (meV) for $\eta = 200$ Å
0	-131.38	-158.33	-173.73
1	-73.13	-113.99	-146.01
2	-45.67	-84.95	-123.87
3	-31.05	-65.30	-106.02

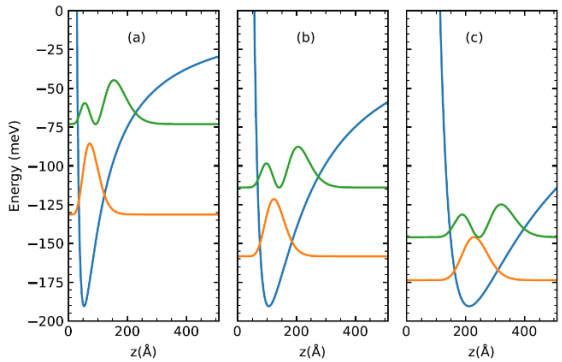

Figure 5 The potential energy profile (blue) and the squared wave functions of the ground (orange) and first excited (green) states of the inversely quadratic Hellmann potential for $U_0 = 300$ meV and (a) $\eta = 50$ Å , (b) $\eta = 100$ Å and (c) $\eta = 200$ Å

3.6 Kratzer-Fues Potential

This potential is particularly useful in molecular spectroscopy for analyzing vibrational-rotational spectra of diatomic molecules. It finds applications in studying bonding properties and bond dissociation energies, making it essential for chemical reaction dynamics and understanding molecular stability. It is derived by Kratzer and Fues as a combination of a Coulomb potential and an inverse-square potential (Kratzer, 1920; Fues, 1926). The specific shape of this potential well holds significant importance for accurately determining vibrational and rotational energy eigenvalues (Bayrak et al., 2006; Khordad, 2013; Dehyar et al., 2016).

The Kratzer-Fues potential is given as

$$U(z) = -U_0\left(\frac{2r_0}{z} - \frac{r_0^2}{z^2}\right) \qquad (16)$$

where U_0 and r_0 are constants (Ungan et al., 2019). The potential minimum is $U_{min} = -U_0$ at $z_{min} = r_0$. The well width and depth are scaled with r_0 and U_0, respectively. The potential energy profile and the squared wave functions of the ground and first excited states are shown in Figure 6 for $U_0 = 300$ meV and for $r_0 = 50$ Å, for $r_0 = 100$ Å and for $r_0 = 200$ Å. The z values is taken until 10^4 Å in the calculations because of the horizontal asymptote at $U = 0$. Energy values of the bounded states are given in Table 6. As the parameter r_0 increases, the potential energy profile expands. Consequently, the energy values of the lowest two subbands approach each other; the transition energy between them decreases from 79.72 meV to 33.84 meV.

Table 6. Energy values of the Kratzer-Fues potential for $U_0 = 300$ meV and for $r_0 = 50$ Å, $r_0 = 100$ Å and $r_0 = 200$ Å

n	E_n (meV) for $r_0 = 50$ Å	E_n (meV) for $r_0 = 100$ Å	E_n (meV) for $r_0 = 200$ Å
0	-227.99	-261.44	-280.05
1	-148.27	-205.29	-246.21
2	-104.08	-165.46	-218.15
3	-77.06	-136.19	-194.63

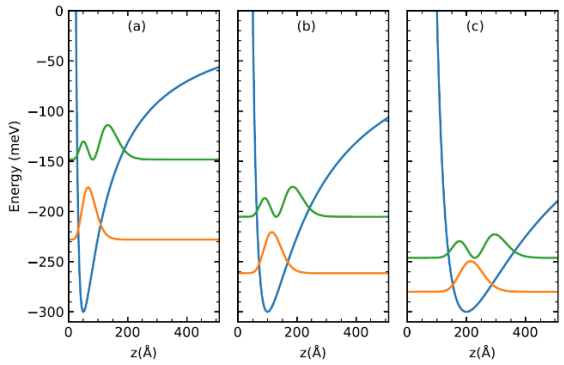

Figure 6 The potential energy profile (blue) and the squared wave functions of the ground (orange) and first excited (green) states of the Kratzer-Fues potential for $U_0 = 300$ meV and for (a) $r_0 = 50$ Å, (b) $r_0 = 100$ Å and (c) $r_0 = 200$ Å

3.7 Morse Potential

The Morse potential is widely used in molecular physics to model the bonding and vibration of diatomic molecules. It is crucial in calculating spectroscopic constants, studying chemical bonds, and even in designing materials with tailored properties, as it provides insights into bond strength and energy dissociation. Morse initially introduced this potential as a valuable model for diatomic molecules, offering a more accurate depiction of the potential energy compared to the quantum harmonic oscillator (Morse, 1929). This potential proves valuable, as anharmonic potentials are frequently essential for mathematically modeling various physical phenomena (Nieto and Simmons, 1979; Duru, 1983; Costa Filho et al., 2013).

The Morse potential is given as

$$U(z) = U_0 \left[\exp\left(-\frac{2z}{\eta}\right) - 2\exp\left(-\frac{z}{\eta}\right)\right] \quad (17)$$

where U_0 and η are constants (Sakiroglu et al., 2016; Ungan et al., 2021). The potential minimum is $U_{min} = -U_0$ at $z_{min} = 0$. The well width and depth are scaled with η and U_0, respectively. The potential energy profile and the squared wave functions of the ground and first excited states are shown in Figure 7 for $U_0 = 300$ meV and for $\eta = 50$ Å, $\eta = 100$ Å and $\eta = 200$ Å. The z values is taken until 10^4 Å in the calculations because of the horizontal asymptote at $U = 0$. Energy values of the bounded states are given in Table 7. As the parameter η increases, the potential energy profile expands. Consequently, the energy values of the lowest two subbands approach each other; the transition energy between them decreases from 119.71 meV to 38.45 meV.

Table 7. Energy values of the Morse potential for $U\_0 = 300$ meV and for $\eta = 50$ "Å" , $\eta = 100$ "Å" and $\eta = 200$ Å

n	E_n (meV) for $\eta = 50$ Å	E_n (meV) for $\eta = 100$ Å	E_n (meV) for $\eta = 200$ Å
0	-223.09	-260.12	-279.70
1	-103.38	-188.89	-241.25
2	-29.15	-129.04	-205.63
3	-0.40	-80.55	-172.86

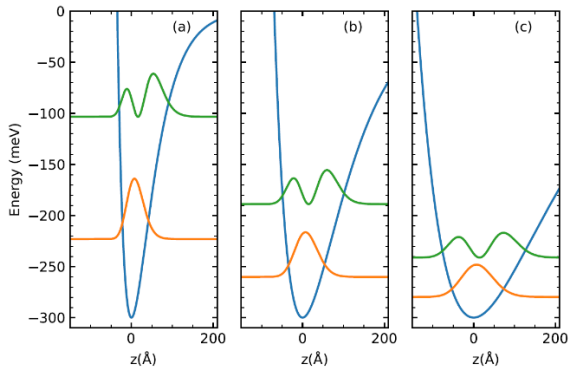

Figure 7. The potential energy profile (blue) and the squared wave functions of the ground (orange) and first excited (green) states of the Morse potential for $U_0 = 300\,meV$ and for (a) $\eta = 50$ Å, (b) $\eta = 100$ Å and (c) $\eta = 200$ Å

3.8 Absorption Coefficients

The absorption coefficients of these quantum potentials are crucial because each potential models specific molecular, atomic, or nuclear interactions, making them ideal for applications requiring precise energy interaction data. Their unique characteristics enable tailored molecular and material design in fields like optics and photodetectors, enhance the accuracy of spectroscopic analysis, and support quantum and nanoscale devices by fine-tuning energy absorption properties. Additionally, they aid efficient energy transfer for thermal management and improve medical imaging and phototherapy by ensuring controlled interactions with radiation. This specificity makes these coefficients invaluable for designing advanced technologies across various fields.

For the calculations of the absorption coefficients, we used $\sigma_s = 3 \times 10^{22}\ \mathrm{m}^{-3}$, $\hbar\Gamma_0 = 60$ meV and $n_r = 3.2$. Figure 8 illustrates the linear optical absorption coefficients concerning optical transitions between the ground and the first-excited states, plotted against the incident photon energy. The maxima in the absorption spectra for the Rosen-Morse and the Pöschl-Teller potentials stay nearly constant when the related parameters of the potentials are subjected to change. However, the maxima in the absorption spectra for the rest of the potential functions either decrease or increase following the changes in the parameters. Regarding the transition energy, it can be said that the potential energy profiles with the current parameters yield values ranging from the lower limit of near-infrared region, for example 423.67 meV in the case of the Rosen-Morse potential, to the middle of the far-infrared region, for example 62.08 meV in the case of the Razavy potential, as shown in Table 8. In terms of wavelength, the calculated values give us a range between 102.44 and 15.01 THz. Generally speaking, the last three potential profiles, namely the Hellmann, Kratzer-Fues and Morse, yield transition energies near the lower limit of the mid-infrared range, while the Rose-Morse potential profile give values close to the upper limit. On the other hand, the remaining profiles provide transition energy values around the middle part of the mid-infrared region. For the double well of the Razavy potentail, the absorptions at the transition energies $E_{10} = E_1 - E_0$ and $E_{21} = E_2 - E_1$ are calculated, as seen in Figure 8.

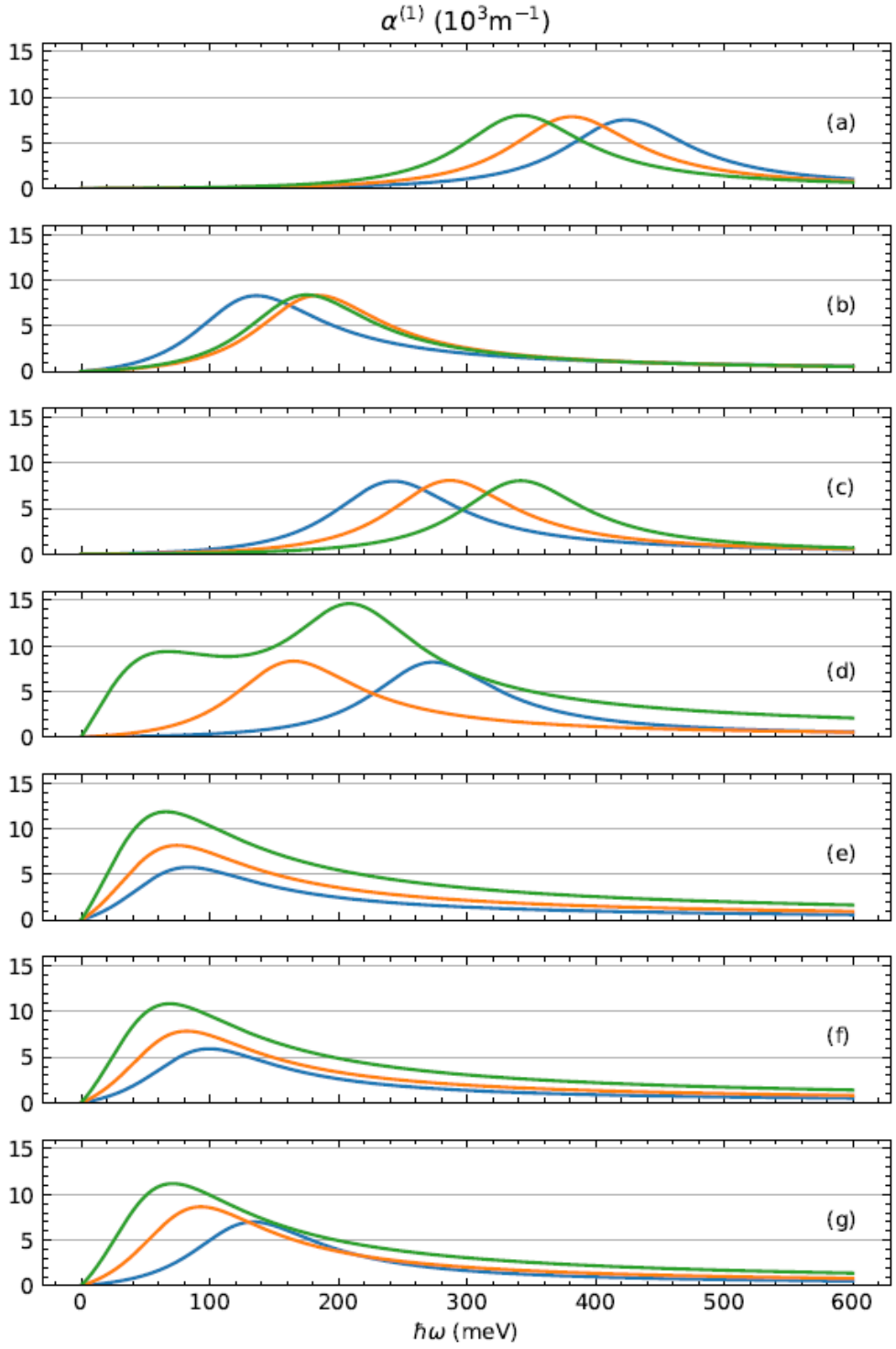

Figure 8. The linear absorption coefficients of (a) the Rosen-Morse potential for $\eta = 20$ Å (blue), $\eta = 25$ Å (orange) and $\eta = 30$ Å (green), (b) the Wood-Saxon potential for $\gamma = 0.1$ Å (blue), for $\gamma = 10$ Å (orange) and for $\gamma = 20$ Å (green), (c) the Pöschl-Teller potential for $k = 1.2$ (blue), $k = 2$ (orange) and $k = 3$ (green), (d) the Razavy potential for $M = 1$ (blue), $M = 2$ (orange) and $M = 3$ (green), and (e) the inversely quadratic Hellmann potential $\eta = 50$ Å (blue), $\eta = 100$ Å (orange) and $\eta = 200$ Å (green), (f) the Kratzer-Fues potential for $r_0 = 50$ Å (blue), $r_0 = 100$ Å (orange) and $r_0 = 200$ Å (green), and (g) the Morse potential for $\eta = 50$ Å (blue), $\eta = 100$ Å (orange) and $\eta = 200$ Å (green)

Table 8. Absorption coefficients and transition energies

Rosen-Morse potential for $U_0 = 835.49$ meV		
$\eta = 20$ Å	$\hbar\omega = 423.67$ (meV) $= 102.44$ (THz)	$\alpha^{(1)}(\hbar\omega) = 7.55 \times 10^3 \mathrm{m}^{-1}$
$\eta = 25$ Å	$\hbar\omega = 381.58$ (meV) $= 92.27$ (THz)	$\alpha^{(1)}(\hbar\omega) = 7.90 \times 10^3 \mathrm{m}^{-1}$
$\eta = 30$ Å	$\hbar\omega = 342.70$ (meV) $= 82.86$ (THz)	$\alpha^{(1)}(\hbar\omega) = 8.04 \times 10^3 \mathrm{m}^{-1}$
Wood-Saxon potential for $U_0 = 835.49$ meV and $Z_0 = 50$ Å		
$\gamma = 0.1$ Å	$\hbar\omega = 136.41$ (meV) $= 32.98$ (THz)	$\alpha^{(1)}(\hbar\omega) = 8.32 \times 10^3 \mathrm{m}^{-1}$
$\gamma = 10$ Å	$\hbar\omega = 184.06$ (meV) $= 44.51$ (THz)	$\alpha^{(1)}(\hbar\omega) = 8.35 \times 10^3 \mathrm{m}^{-1}$
$\gamma = 20$ Å	$\hbar\omega = 175.54$ (meV) $= 42.45$ (THz)	$\alpha^{(1)}(\hbar\omega) = 8.40 \times 10^3 \mathrm{m}^{-1}$
Pöschl-Teller potential for $L = 100$ Å and $\eta = 2$		
$k = 1.2$	$\hbar\omega = 243.00$ (meV) $= 58.76$ (THz)	$\alpha^{(1)}(\hbar\omega) = 8.02 \times 10^3 \mathrm{m}^{-1}$
$k = 2$	$\hbar\omega = 286.80$ (meV) $= 69.35$ (THz)	$\alpha^{(1)}(\hbar\omega) = 8.10 \times 10^3 \mathrm{m}^{-1}$
$k = 3$	$\hbar\omega = 341.84$ (meV) $= 82.66$ (THz)	$\alpha^{(1)}(\hbar\omega) = 8.07 \times 10^3 \mathrm{m}^{-1}$
Razavy potential for $U_0 = 300$ meV, $D = 50$ Å and $A = 2$		
$M = 1$	$\hbar\omega = 273.81$ (meV) $= 66.21$ (THz)	$\alpha^{(1)}(\hbar\omega) = 8.23 \times 10^3 \mathrm{m}^{-1}$
$M = 2$	$\hbar\omega = 165.16$ (meV) $= 39.94$ (THz)	$\alpha^{(1)}(\hbar\omega) = 8.34 \times 10^3 \mathrm{m}^{-1}$
$M = 3$	$\hbar\omega = 62.08$ (meV) $= 15.01$ (THz)	$\alpha^{(1)}(\hbar\omega) = 8.88 \times 10^3 \mathrm{m}^{-1}$
$M = 3$	$\hbar\omega = 212.14$ (meV) $= 55.00$ (THz)	$\alpha^{(1)}(\hbar\omega) = 10.47 \times 10^3 \mathrm{m}^{-1}$
The inversely quadratic Hellmann potential for $U_0 = 300$ meV		
$\eta = 50$ Å	$\hbar\omega = 83.63$ (meV) $= 20.22$ (THz)	$\alpha^{(1)}(\hbar\omega) = 5.79 \times 10^3 \mathrm{m}^{-1}$
$\eta = 100$ Å	$\hbar\omega = 74.61$ (meV) $= 18.04$ (THz)	$\alpha^{(1)}(\hbar\omega) = 8.18 \times 10^3 \mathrm{m}^{-1}$
$\eta = 200$ Å	$\hbar\omega = 66.09$ (meV) $= 15.98$ (THz)	$\alpha^{(1)}(\hbar\omega) = 11.87 \times 10^3 \mathrm{m}^{-1}$
Kratzer-Fues potential for $U_0 = 300$ meV		
$r_0 = 50$ Å	$\hbar\omega = 99.78$ (meV) $= 24.13$ (THz)	$\alpha^{(1)}(\hbar\omega) = 5.93 \times 10^3 \mathrm{m}^{-1}$
$r_0 = 100$ Å	$\hbar\omega = 82.18$ (meV) $= 19.87$ (THz)	$\alpha^{(1)}(\hbar\omega) = 7.86 \times 10^3 \mathrm{m}^{-1}$
$r_0 = 200$ Å	$\hbar\omega = 68.88$ (meV) $= 16.66$ (THz)	$\alpha^{(1)}(\hbar\omega) = 10.87 \times 10^3 \mathrm{m}^{-1}$
Morse potential for $U_0 = 300$ meV		
$\eta = 50$ Å	$\hbar\omega = 133.91$ (meV) $= 32.38$ (THz)	$\alpha^{(1)}(\hbar\omega) = 6.99 \times 10^3 \mathrm{m}^{-1}$
$\eta = 100$ Å	$\hbar\omega = 93.13$ (meV) $= 22.52$ (THz)	$\alpha^{(1)}(\hbar\omega) = 8.65 \times 10^3 \mathrm{m}^{-1}$
$\eta = 200$ Å	$\hbar\omega = 71.27$ (meV) $= 17.23$ (THz)	$\alpha^{(1)}(\hbar\omega) = 11.19 \times 10^3 \mathrm{m}^{-1}$

4. Conclusion

In this work, we have studied the GaAs/AlGaAs quantum well for several bounded potentials, and the intersubband absorption coefficients of the transition energies are presented for different well parameters. The potential functions are Rosen-Morse, Wood-Saxon, Pöschl-Teller, Razavy, inversely quadratic Hellmann,

Kratzer-Fues and Morse potentials. The transition energies of absorption coefficients vary according to well parameters, from the lower limit of near-infrared to the middle of the far-infrared region.

The findings of this study provide a foundation for optimizing the characteristics of GaAs/AlGaAs quantum well structures, aiding in their application across a wide range of technologies, including semiconductor lasers, photodetectors, and quantum cascade devices. Each potential has distinct uses, but collectively, they contribute to fields such as quantum mechanics, molecular chemistry, condensed matter physics, and nanotechnology. The detailed analysis of how each potential impacts transition energies and absorption characteristics enables a refined approach to tuning quantum wells for specific optical and electronic responses, which is essential for advancing infrared sensing and telecommunications applications. We believe that the results of the present study will be helpful to researchers in designing possible quantum optoelectronic devices, providing a roadmap for selecting and customizing potential models to achieve the desired operational parameters in real-world applications.

Author Contribution

Tərlan ZƏRBALİYEV: Data Collection and Analysis, Literature Review
Raşit ÇAKIR: Supervision, Software, Formal analysis, Data Curation, Visualization, Writing - Original Draft
Hasan YILDIRIM: Methodology, Validation, Review and Editing,

Funding Statement

The authors declare that they have no known competing financial interests or personal relationships that could have appeared to influence the work reported in this paper.

Conflict of Interest Statement

We declare that there is no conflict of interest regarding the publication of this article.

Ethical Standards

No Ethics Committee Approval is required for this study

References

Ahn, D. and Chuang, S.-l. (1987). Calculation of linear and nonlinear intersubband optical absorptions in a quantum well model with an applied electric field. *IEEE Journal of Quantum Electronics,* 23(12), 2196-2204. https://doi.org/10.1109/JQE.1987.1073280

Atić, A., Vuković, N. and Radovanović, J. (2022.) Calculation of intersubband absorption in ZnO/ZnMgO asymmetric double quantum wells. *Optical and Quantum Electronics,* 54, 810. https://doi.org/10.1007/s11082-022-04170-0

Atić, A., Wang X., Vuković, N., Stanojević N., Demić A., Indjin D. and Radovanović J. (2024). Resonant Tunnelling and Intersubband Optical Properties of ZnO/ZnMgO Semiconductor Heterostructures: Impact of Doping and Layer Structure Variation. *Materials, 17*(4), 927. https://doi.org/10.3390/ma17040927

Aytekin, O., Turgut, S. and Tomak, M. (2012). Nonlinear optical properties of a Pöschl–Teller quantum well under electric and magnetic fields. *Physica E: Low-dimensional Systems and Nanostructures,* 44, 1612–1616. https://doi.org/10.1016/j.physe.2012.04.005

Bayrak, O., Boztosun, I. and Ciftci, H. (2006). Exact analytical solutions to the Kratzer potential by the asymptotic iteration method. *International Journal of Quantum Chemistry,* 107, 540-544. https://doi.org/10.1002/qua.21141

Cominotti, R. and Leymann, H. A. M. and Nespolo, J. and Manceau, J.-M. and Jeannin, M. and Colombelli, R. and Carusotto, I. (2023). Theory of coherent optical nonlinearities of intersubband transitions in semiconductor quantum wells. *Physical Review B*, 107(11), 115431. https://doi.org/10.1103/PhysRevB.107.115431

Costa Filho, R.N., Alencar, G., Skagerstam, B.S. and Andrade jr, J.S. (2013). Morse potential derived from first principles. Europhysics Letters, 101(1), 10009. https://doi.org/10.1209/0295-5075/101/10009

Dehyar, A., Rezaei, G. and Zamani, A. (2016). Electronic structure of a spherical quantum dot: Effects of the Kratzer potential, hydrogenic impurity, external electric and magnetic fields. *Physica E: Low-dimensional Systems and Nanostructures*, 84, 175-181. https://doi.org/10.1016/j.physe.2016.05.038

Duan, Y., Li, X., Chang, C., Zhao, Z. and Zhang, L. (2022). Hydrostatic pressure, temperature and Al-concentration effects on optical rectification of spherical quantum dots under inversely quadratic Hellmann potential. *Optik*, 254, 168596. https://doi.org/10.1016/j.ijleo.2022.168596

Duru, I.H. (1983). Morse-potential Green's function with path integrals. *Physical Review D*, 28, 2689. https://doi.org/10.1103/PhysRevD.28.2689.

Falaye, B.J. (2012). Energy spectrum for trigonometric Pöschl-Teller potential. *Canadian Journal of Physics*, 90(12), 1259-1265. https://doi.org/10.1139/p2012-103

Finkel, F., González-López, A. and Rodrígue, M.A. (1999). On the families of orthogonal polynomials associated to the Razavy potential. *Journal of Physics A: Mathematical and General*, 32(29), 6821-6835. https://doi.org/10.1088/0305-4470/32/39/308

Flügge, S. (1999). Practical Quantum Mechanics. Springer Berlin, ISBN: 978-3-540-65035-5, Heidelberg, Germany. https://doi.org/10.1007/978-3-642-61995-3

Fues, E. (1926). Das eigenschwingungsspektrum zweiatomiger moleküle in der undulationsmechanik. *Annalen der Physik*, 385, 367-396. https://doi.org/10.1002/andp.19263851204

Ghanbari, A. (2023). Studying third harmonic generation in spherical quantum dot under inversely quadratic Hellmann potential. *Optical and Quantum Electronics*, 55, 222. https://doi.org/10.1007/s11082-022-04513-x

Haghighatzadeh, A. and Attarzadeh, A. (2023). A comprehensive investigation on valence-band electronic structure and linear and nonlinear optical properties of a laser-driven GaAsSb-based Rosen-Morse quantum well. *The European Physical Journal B*, 96, 125. https://doi.org/10.1140/epjb/s10051-023-00592-1

Hamzavi, M. and Rajabi, A. (2011). Exact s-wave solution of the trigonometric pöschl-teller potential. *International Journal of Quantum Chemistry*, 112, 1592–1597. https://doi.org/10.1002/qua.23166

Harrison, P. (2005). Numerical Solutions. In: *Quantum Wells, Wires and Dots: Theoretical and Computational Physics of Semiconductor Nanostructures* (Eds. Harrison, P. and Valavanis, A), John Wiley and Sons Ltd. ISBN:9780470010792, Chichester, England. http://doi.org/10.1002/0470010827

Hellmann, H. (1936). Ein kombiniertes Näherungsverfahren zur Energieberechnung im Vielelektronenproblem. II. *Acta Physicochim. USSR*, 4, 225-244.

Kasapoglu, E., Sarı, H., Sökmen, I., Vinasco, J.A., Laroze, D. and Duque, C.A. (2021). Effects of intense laser field and position dependent effective mass in Razavy quantum wells and quantum dots. *Physica E: Low-dimensional Systems and*

Nanostructures, 126, 114461. https://doi.org/10.1016/j.physe.2020.114461

Khordad, R. (2013). Confinement of an exciton in a quantum dot: Effect of modified Kratzer potential. *Indian Journal of Physics*, 87, 623–628. https://doi.org/10.1007/s12648-013-0281-9

Khordad, R. and Mirhosseini, B. (2014). Linear and nonlinear optical properties in spherical quantum dots: Rosen–Morse potential. *Condenced-Matter Spectroscopy*, 117(3), 434-440. https://doi.org/10.1134/S0030400X14090100

Khurgin, J.B. (2023). Basic Physics of Intersubband Radiative and Nonradiative Processes. In: *Mid-Infrared and Terahertz Quantum Cascade Lasers* (Eds. Botez, D. and Belkin, A.M.), Cambridge University Press. ISBN: 9781108552066. https://doi.org/10.1017/9781108552066

Kratzer, A. (1920). Die ultraroten Rotationsspektren der Halogenwasserstoffe. *Zeitschrift für Physik*, 3, 289–307. https://doi.org/10.1007/BF01327754

Máthé, L., Onyenegecha, C.P., Farcaş, A.-A., Pioraş-Ţimbolmaş, L.-M., Solaimani, M. and Hassanabadi, H. (2021). Linear and nonlinear optical properties in spherical quantum dots: Inversely quadratic Hellmann potential. *Physics Letters A*, 397, 127262. https://doi.org/10.1016/j.physleta.2021.127262

Morse, P.M. (1929). Diatomic Molecules According to the Wave Mechanics. II. Vibrational Levels. *Physical Review*, 34, 57-64. https://doi.org/10.1103/PhysRev.34.57

Nieto, M.M. and Simmons Jr., L.M. (1979). Eigenstates, coherent states, and uncertainty products for the Morse oscillator. *Physical Review A*, 19(2), 438-444. https://doi.org/10.1103/PhysRevA.19.438

Njoku, I.J., Onyenegecha, C.P., Okereke, C.J., Nwaokafor, P. and Abara, C.C. (2023). Relativistic energies and information entropy of the inversely quadratic Hellmann potential. *Physics Open*, 15, 100152. https://doi.org/10.1016/j.physo.2023.100152

Persichetti, L., Montanari, M., Ciano, C., Di Gaspare, L., Ortolani, M., Baldassarre, L., Zoellner, M., Mukherjee, S., Moutanabbir, O., Capellini, G., Virgilio, M., and De Seta, M. (2020). Intersubband Transition Engineering in the Conduction Band of Asymmetric Coupled Ge/SiGe Quantum Wells. *Crystals*, 10(3), 179. https://doi.org/10.3390/cryst10030179

Pöschl, G. and Teller, E. (1933). Bemerkungen zur Quantenmechanik des anharmonischen Oszillators. *Zeitschrift für Physik*, 83, 143–151. https://doi.org/10.1007/BF01331132

Razavy, M. (1980). An exactly soluble Schrödinger equation with a bistable potential. *American Journal of Physics*, 48(4), 285-288. https://doi.org/10.1119/1.12141

Restrepo, R.L., Morales, A.L., Akimov, V., Tulupenko, V., Kasapoglu, E., Unfan F. and Duque C.A. (2015). Intense laser field effects on a Woods–Saxon potential quantum well. *Superlattices and Microstructures*, 87, 143-148. https://doi.org/10.1016/j.spmi.2015.03.070

Rosen, N. and Morse, P.M. (1932). On the Vibrations of Polyatomic Molecules. *Physical Review*, 42, 210-217. https://doi.org/10.1103/PhysRev.42.210

Sakiroglu, S., Kasapoglu, E., Restrepo, R.L., Duque, C.A. and Sökmen, I. (2016). Intense laser field-induced nonlinear optical properties of Morse quantum well. *Physica Status Solidi B*, 254(4), 1600457. https://doi.org/10.1002/pssb.201600457

Salman Durmuslar, A., Turkoglu, A., Mora-Ramos, M.E. and Ungan, F. (2022). The non-resonant intense laser field effects on the binding energies and the nonlinear optical properties of a donor impurity in Rosen-Morse quantum well. *Indian Journal of Physics*, 96(12), 3485–3492.

https://doi.org/10.1007/s12648-021-02251-6

Sayrac, M., Peter, A.J. and Ungan, F. (2022). Interband transitions and exciton binding energy in a Razavy quantum well: effects of external fields and Razavy potential parameters. *The European Physical Journal Plus*, 137, 840. https://doi.org/10.1140/epjp/s13360-022-03038-2

Sous, A.J. (2007). Eigenenergies for the Razavy potential $V(x) = (\zeta \cosh 2x\text{-}M)^2$ using the asymptotic iteration method. *Modern Physics Letters A*, 22(22), 1677-1684. https://doi.org/10.1142/S0217732307021433

Turkoglu, A., Dakhlaoui, H., Durmuslar, A.S., Mora-Ramos, M.E. and Ungan, F. (2021). Nonlinear optical properties of a quantum well with inversely quadratic Hellman potential. *The European Physical Journal B*, 94, 111. https://doi.org/10.1140/epjb/s10051-021-00129-4

Ungan, F. and Bahar, M.K. (2019). Optical specifications of laser-induced Rosen-Morse quantum well. *Optical Materials*, 90, 231-237. https://doi.org/10.1016/j.optmat.2019.02.040

Ungan, F. and Bahar, M.K. (2020). The laser field controlling on the nonlinear optical specifications of the electric field-triggered Rosen-Morse quantum well. *Physics Letters A*, 384(19), 126400. https://doi.org/10.1016/j.physleta.2020.126400

Ungan, F., Bahar, M.K., Barseghyan, M.G., Pérez, L.M. and Laroze, D. (2021). Effect of intense laser and electric fields on nonlinear optical properties of cylindrical quantum dot with Morse potential. *Optik*, 236, 166621. https://doi.org/10.1016/j.ijleo.2021.166621

Ungan, F., Martínez-Orozco, J.C., Restrepo, R.L. and Mora-Ramos, M.E. (2019). The nonlinear optical properties of GaAs-based quantum wells with Kratzer–Fues confining potential: Role of applied static fields and non-resonant laser radiation. *Optik*, 185, 881-887. https://doi.org/10.1016/j.ijleo.2019.03.129

Ungan, F., Mora-Ramos, M.E., Yesilgul U., Sari, H. and Sökmen, I. (2019). Effect of applied external fields on the nonlinear optical properties of a Woods-Saxon potential quantum well. *Physica E: Low-dimensional systems and nanostructures*, 111, 167-171. https://doi.org/10.1016/j.physe.2019.03.015

van der Walt, S., Colbert, S.C., and Varoquaux, G. (2011). The numpy array: A structure for efficient numerical computation. *Computing in Science and Engineering*, 13(2), 22-30. https://doi.org/10.1109/MCSE.2011.37

Woods, R.D. and Saxon, D.S. (1954). Diffuse surface optical model for nucleon-nuclei scattering. *Physical Review*, 95, 577-578. https://doi.org/10.1103/PhysRev.95.577

Xie, W. (2009). A study of two confined electrons using the Woods–Saxon potential. *Journal of Physics: Condensed Matter*, 21(11), 115802. https://doi.org/10.1088/0953-8984/21/11/115802

Yıldırım, H. and Tomak, M. (2005). Nonlinear optical properties of a Pöschl-Teller quantum well. *Physical Review B*, 72, 115340. https://doi.org/10.1103/physrevb.72.115340

Yildirim, H. and Tomak, M. (2006). Intensity-dependent refractive index of a Pöschl-Teller quantum well. *Journal of Applied Physics*, 99, 093103. https://doi.org/10.1063/1.2194124